Title

Gull-inspired joint-driven wing morphing allows adaptive longitudinal flight control

Journal

Journal of The Royal Society Interface, 18(179)

ISSN

1742-5689

Authors

Harvey, C
Baliga, VB
Goates, CD
et al.

Publication Date

2021-06-01

DOI

10.1098/rsif.2021.0132

Peer reviewed

INTERFACE

royalsocietypublishing.org/journal/rsif

Research

Cite this article: Harvey C, Baliga VB, Goates CD, Hunsaker DF, Inman DJ. 2021 Gull-inspired joint-driven wing morphing allows adaptive longitudinal flight control. *J. R. Soc. Interface* **18**: 20210132.
https://doi.org/10.1098/rsif.2021.0132

Received: 12 February 2021
Accepted: 17 May 2021

Subject Category:
Life Sciences–engineering interface

Subject Areas:
biomechanics, biomimetics

Keywords:
wing morphing, biomechanics, gliding flight, wind tunnel, MachUpX

Author for correspondence:
C. Harvey
e-mail: harveyca@umich.edu

Electronic supplementary material is available online at https://doi.org/10.6084/m9.figshare.c.5438933.

THE ROYAL SOCIETY PUBLISHING

Gull-inspired joint-driven wing morphing allows adaptive longitudinal flight control

C. Harvey[1], V. B. Baliga[2], C. D. Goates[3], D. F. Hunsaker[3] and D. J. Inman[1]

[1]Department of Aerospace Engineering, University of Michigan, Ann Arbor, MI 48109, USA
[2]Department of Zoology, University of British Columbia, Vancouver, BC V6T 1Z4, Canada
[3]Department of Mechanical and Aerospace Engineering, Utah State University, Logan, UT 84322, USA

CH, 0000-0002-2830-0844; VBB, 0000-0002-9367-8974; CDG, 0000-0002-7568-1280; DFH, 0000-0001-8106-7466; DJI, 0000-0001-6195-1334

Birds dynamically adapt to disparate flight behaviours and unpredictable environments by actively manipulating their skeletal joints to change their wing shape. This in-flight adaptability has inspired many unmanned aerial vehicle (UAV) wings, which predominately morph within a single geometric plane. By contrast, avian joint-driven wing morphing produces a diverse set of non-planar wing shapes. Here, we investigated if joint-driven wing morphing is desirable for UAVs by quantifying the longitudinal aerodynamic characteristics of gull-inspired wing-body configurations. We used a numerical lifting-line algorithm (MachUpX) to determine the aerodynamic loads across the range of motion of the elbow and wrist, which was validated with wind tunnel tests using three-dimensional printed wing-body models. We found that joint-driven wing morphing effectively controls lift, pitching moment and static margin, but other mechanisms are required to trim. Within the range of wing extension capability, specific paths of joint motion (trajectories) permit distinct longitudinal flight control strategies. We identified two unique trajectories that decoupled stability from lift and pitching moment generation. Further, extension along the trajectory inherent to the musculoskeletal linkage system produced the largest changes to the investigated aerodynamic properties. Collectively, our results show that gull-inspired joint-driven wing morphing allows adaptive longitudinal flight control and could promote multifunctional UAV designs.

1. Introduction

A bird can begin its day foraging in a slow glide, suddenly needing to evade a predator, only to later fly home battling an incoming storm. The adaptability demonstrated by birds is in part due to their ability to morph the shape of their wings, both actively and passively [1–4]. Previous research has shown that active wing morphing allows birds to dynamically adapt their aerodynamic performance and stability characteristics in response to changing flight conditions or requirements [2,5]. In comparison, fixed-wing unmanned aerial vehicles (UAVs) are often designed to satisfy specific functions, such as high-altitude surveillance or long endurance flights, and efficient operation is limited to their intended mission parameters [6]. The adaptability offered by avian wing morphing is highly desirable for UAVs as it may broaden the efficient operational range, reduce operating costs as well as offer enhanced or novel capabilities [3,6–8]. In addition, UAVs often face aerodynamic control challenges including the need to adapt to variable environmental conditions [9] or manoeuvre through complex territories [10], while birds complete similar tasks with apparent ease. Therefore, it is of no surprise that as engineers strive towards the objective of an adaptive, multifunctional UAV, bird wings have directly and indirectly inspired many morphing wing designs [6,11–15].

The majority of current engineered morphing wings adjust their wing geometry discretely within one or two planes, such as span, sweep, dihedral, etc. [11,12,14,15]. By contrast, bird wings are composed of an underlying musculoskeletal system that can be approximated as a non-planar six-bar linkage

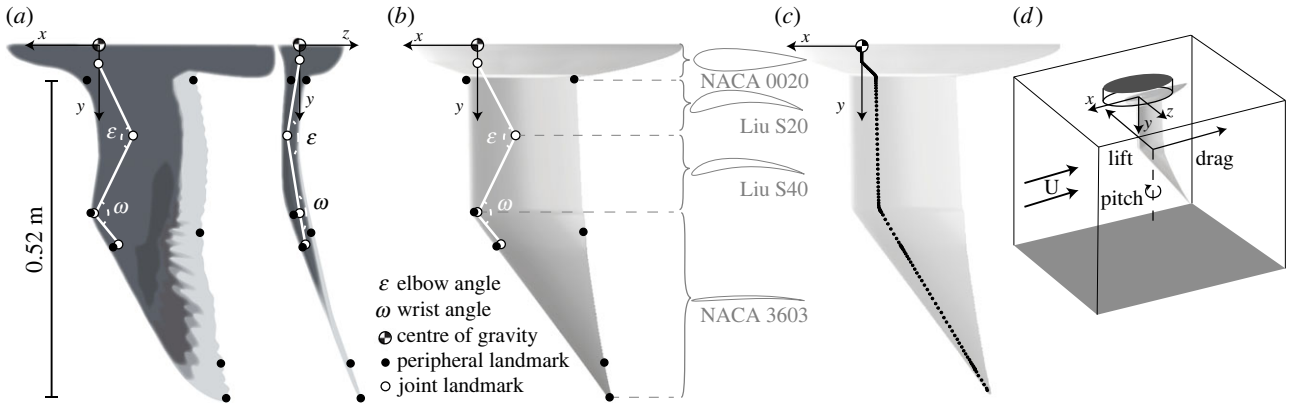

Figure 1. Gull wings inspired our analyses of how avian joint-driven wing morphing affects longitudinal aerodynamic control, stability and balance. (*a*) Wings from gull cadavers ($n = 3$) were manually manipulated throughout the range of motion of the elbow and wrist while tracking the 3D position of seven peripheral landmarks (black points) and four joint landmarks (white points). (*b*) The identified wing shapes were simplified using linear approximations between the peripheral landmarks. Four aerofoils were used to create the wing-body configurations. (*c*) The simplified wing shapes were reflected about the *x*–*z* plane and investigated using MachUpX and cosine clustering to distribute the control points along the span. (*d*) To validate the numerical results, nine wing shapes were 3D printed and tested in a 2 ft-by-2 ft low-speed wind tunnel.

system [16]. When the applicable muscles are activated, the non-planar musculoskeletal linkage causes three-dimensional (3D) changes to the overall wing geometry [5,16,17]. Active manipulation of only two skeletal joints, the elbow and wrist is responsible for the majority of this wing shape change (figure 1) [5,17]. These joints have three degrees of freedom, i.e. the ability to extend/flex, pronate/supinate and elevate/depress [17]. However, within gliding flight extension/flexion dominates the range of motion and thus we have limited our study to focus only on the range of motion of extension and flexion for the elbow and the wrist (hereafter referred to as 'joint-driven wing morphing'). Therefore, in this work the elbow and the wrist represent an approximated minimum set of coordinates that is required to define the overall wing shape. In this case, traditional geometric properties including distributions of wing twist, sweep, dihedral and the final wingspan can be approximated as functions of the joint positions [5,18]. Further, these non-planar wing shapes likely have aerodynamic characteristics that differ from comparable planar wing aerodynamic theory [19], as highlighted by the Hyper Elliptical Cambered Span (HECS) wing inspired by gulls, which had improved aerodynamic efficiency (higher lift-to-drag ratio) compared to an equivalent planar wing [20].

Despite the physical differences, no engineered morphing wing designs have implemented biologically accurate joint-driven wing morphing. This discrepancy is likely due to the many challenges associated with implementing a non-planar morphing wing including complex manufacturing methods as well as additional mechanism weight and structural rigidity considerations [6]. In addition, because we cannot assume that a bird's wing has been optimized for flight [21], it follows that we cannot assume that a biologically accurate morphing wing will provide any advantage over a planar morphing wing. This leads to the main question of our study: does avian-inspired joint-driven wing morphing provide sufficient aerodynamic benefits to warrant implementation in a future UAV wing design?

To address this question, we investigated the benefits of gull-inspired joint-driven wing morphing by quantifying longitudinal aerodynamic stability and control, which are critical for any successful flight, be it high-altitude surveillance or evasive manoeuvres [4,22,23]. We assumed a symmetric glider with no sideslip, to permit longitudinal (pitch, motion in the *x*–*z* plane, figure 1) and lateral (roll and yaw, motion in the *x*–*y* or *y*–*z* planes) components to be decoupled [22]. In this work, longitudinal control refers to a morphing wing's ability to actively adjust its generated lift force and pitching moment. Traditional aircraft can control lift through wing flap deflections and the pitching moment through elevator deflections [22,23]. In addition to longitudinal control, we considered the effects of joint-driven wing morphing on longitudinal stability and balance. Longitudinal stability is the tendency of an aircraft to return to its equilibrium after an external disturbance, which requires an evaluation of both the static (initial) and dynamic (time-dependent) response [22]. Here, we focused solely on static stability, a necessary but insufficient condition for full stability. Finally, longitudinal balance is the ability for a glider to fly at an equilibrium, also known as trimmed flight.

To quantify the longitudinal control, stability and balance associated with gull-inspired joint-driven wing morphing, we first identified the 3D simplified wing shapes associated with the extension and flexion of the elbow and wrist for hybrid glaucous-winged (*Larus glaucescens*) × western (*Larus occidentalis*) gulls ($n = 3$). We selected gulls as our study species because their non-planar wing shape is known to be actively controlled by elbow and wrist manipulation [5]. In addition, gulls are a good model species for multifunctional UAVs as they are generalist flyers, using a wide variety of flight styles from steady glides to sudden manoeuvres [24,25]. Next, we aligned and simplified each extracted wing shape ($n = 1031$) and connected these wings to a gull-shaped body (figure 1*b*). With each final wing-body configuration, we predicted the aerodynamic properties using MachUpX, a low-order numerical general lifting-line model (figure 1*c*) [26–28]. We validated the outputs from MachUpX with experimental wind tunnel measurements on 3D-printed half-span equivalent wing-body models (figure 1*d*). Finally, we investigated four quasi-steady joint extension trajectories within the range of motion that could be implemented to improve the adaptability of a gull-inspired joint-driven morphing UAV wing.

2. Material and methods

2.1. Determining the wing-body configurations

Wings from gull cadavers ($n = 3$) were manually manipulated throughout their full range of elbow and wrist extension and flexion while filming 11 key landmarks with three high-speed cameras. Seven landmarks on the wing periphery (black points, figure 1*a*) provided an outline of the overall wing shape through the range of motion and four landmarks on the wing joints (white points, figure 1*a*), allowed us to calculate the elbow and wrist angle associated with each wing outline. The videos were digitized using DLTdv5 software [29] to return the 3D position of each landmark. For a detailed methodology on how the 3D landmarks were obtained refer to [5].

The final extracted 3D landmarks were re-oriented using a custom R script to align the wrist joint with the humerus head on the *z*- and *y*-axes (figure 1*b*). We defined 0° angle of attack by rotating the wing about the *y*-axis until the tip of the first secondary feather (S1) was aligned with the wrist joint along the *x*-axis. Next, we exported the aligned landmarks into a custom Python script to ease interfacing with MachUpX and limited the configurations to those with elbow and wrist angles above the minimum angles used *in vivo* by gliding gulls [5]. Next, the wings were segmented along the *x*-axis at each peripheral landmark. For each segment, the custom script returned simplified leading and trailing edge points, and a value of sweep, dihedral and twist within that segment. The last 5% of the wing segment span was linearly blended into the next segment to avoid sharp changes in wing geometry. These geometric properties were selected to minimize error between the true peripheral landmarks and the final simplified wing shapes. The maximum summed error for all landmarks was found to be 2.1 mm.

Next, we selected three aerofoils to distribute along the wingspan. We extracted two aerofoils from a previously published scan of a gull wing at 20% (Liu S20) and 40% (LiuS20) span (figure 1*b*) [30]. As the species was not identified in that study, we assumed that the aerofoil shape is similar between different gull species. We defined the aerofoils for each segment based on the locations of the skeletal joints as illustrated in figure 1*b*. For segments more distal than the wrist joint, we assigned a NACA 3603 aerofoil because the scan did not capture the wing after 77.2% span [30]. We selected the NACA 3603 after compiling a list of measured distal avian aerofoils [31–33]. All aerofoils were linearly blended to create a smooth wing surface within the MachUpX framework [26].

There are a few key assumptions on the final wing shapes. First, we assumed that throughout elbow and wrist extension and flexion, the digits (including the alula) remain fixed. Next, we elected to not consider the capability to elevate/depress or supinate/pronate along joints within the wing or to adjust overall wing position via rotation at the shoulder joint. Additionally, we neglected wing porosity, roughness and flexibility to isolate the effects solely due to the shape change created by joint-driven wing morphing. Owing to these assumptions and the alignment routine, the final wing shapes are not necessarily representative of an in-flight configuration used by live gulls.

Each final wing shape was attached to a gull-inspired body. We selected a NACA0020 aerofoil based on an estimated body length (41 cm) and body height that was estimated using an allometric relationship with a body mass of 0.91 kg [34,35]. The shoulder joint was positioned at the quarter-chord of the body. The body width and position of the shoulder joint along the *y*-axis (figure 1*b*) was determined from allometric relationships with the same body mass [35]. To create an avian-like body shape, we reduced the body chord from a maximum at the body's centre to the wing root chord length at the body's edges using a cosine distribution.

For each wing-body configuration, we quantified a few traditional geometric properties including the total and projected wing area, as well as wing tip twist, sweep and dihedral (figure 3*c*). The total wing area is half of the entire wing-body wetted surface area where the projected wing area is the wing-only area projected onto the *y*–*x* plane at 0°, the body projected area remains approximately constant. The wing tip twist, dihedral and sweep values were calculated for the most distal wing segment within our custom Python script. Note that all tested wing shapes had wingtips with some degree of backwards sweep and anhedral.

2.2. Numerical lifting-line solution (MachUpx)

MachUpX is a Python implementation of the Goates–Hunsaker (G-H) general numerical lifting-line method, which is a modern extension of Prandtl's classical lifting-line theory [26–28]. Within the G-H method, the wing is replaced by a set of horseshoe vortices and Prandtl's lifting-line hypothesis is enforced at a single control point on each vortex to determine the aerodynamics of the wing. Wings are modelled in MachUpX using the quarter-chord distribution of sweep, dihedral and twist. Multiple spanwise sections can also be used to incorporate viscous effects by allowing for viscous section lift, drag and moment coefficients. The outputs from MachUpX used in this study are the total forces and moments for a given wing-body configuration. As a low-order numerical method, MachUpX is ideal for quickly performing comprehensive investigations of multi-degree-of-freedom design spaces.

We evaluated the wings as a symmetric full-span configuration at a velocity (U) of $10\ \mathrm{m\ s^{-1}}$ to approximate a gull's gliding speed (density (ρ): $1.225\ \mathrm{kg\ m^{-3}}$, kinematic viscosity: $1.81 \times 10^{-5}\ \mathrm{m^2\ s^{-1}}$) [5,36]. We specified a grid resolution of 200 cosine clustered vortices for the wing and 60 for the body (figure 1*c*). We used MachUpX's nonlinear solver with a convergence tolerance of 10^{-6} and a relaxation factor of 1, 0.8, 0.5 or 0.01. Each wing was tested from –10° to 10° in increments of 1°. In total, we had convergence for at least one angle of attack for 1031 wing-body configurations with a total of 9720 converged test cases. The majority of the convergence was at lower angles of attack.

We used the MachUpX outputs to investigate the lift and pitching moment for the wing-body configurations. We were not able to investigate the maximum lift produced by each configuration due to the limitations of the numerical method for the complex shapes. Additionally, we did not investigate drag as it was outside the scope of this study, but it likely plays a variable role in avian wing morphing and warrants future investigation. Note that MachUpX predicted the experimental drag within the expanded experimental uncertainty range for all wings except for configurations 6, 7, 8 and 9 (figure 2*c*).

To allow comparison between the experimental and numerical lift and pitching moments, we non-dimensionalized the outputs by the dynamic pressure ($1/2\rho U^2$), maximum total wing area ($S_{\max}$) and maximum wing-body mean chord ($c_{\max}$) for each specimen across all morphed configurations to obtain $C_{L_{\mathrm{morph}}}$ and $C_{m_{\mathrm{morph}}}$, respectively. These adjusted aerodynamic coefficients allow comparisons across different wing specimens without filtering out the wing area change due joint-driven wing morphing. As there is relatively little information about the location of a bird's centre of gravity, we evaluated the pitching moment about the body's quarter-chord (aligned with the shoulder joint); this effectively assumes that the centre of gravity is located at the body's quarter-chord (figure 1*a*).

2.3. Wind tunnel study

To validate the numerical results from MachUpX, we 3D-printed nine wing-body configurations across the range of motion

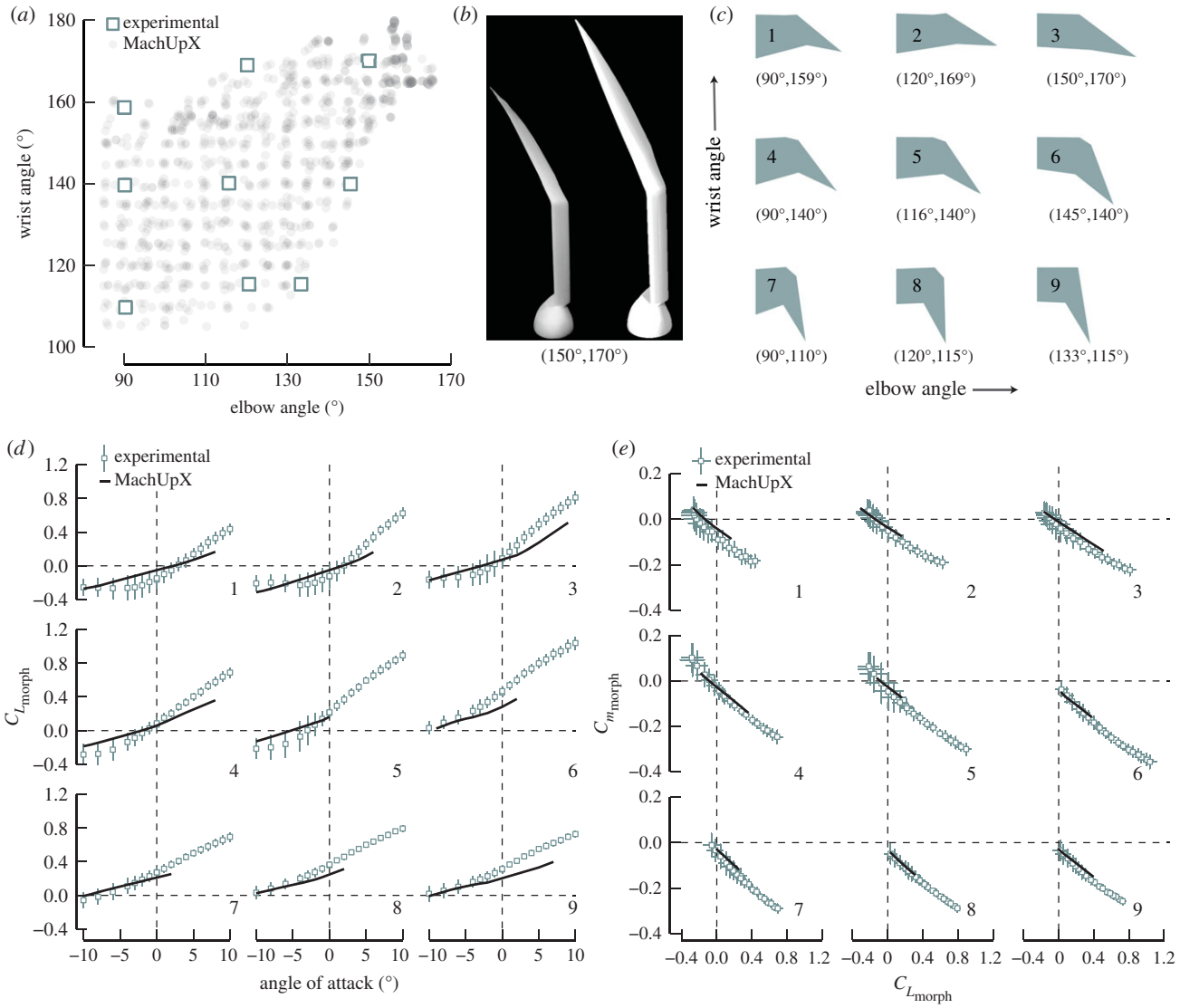

Figure 2. MachUpX effectively predicted the aerodynamic forces and moments for the investigated wing shapes. (*a*) The *in vivo* range of motion used by gliding gulls was investigated using MachUpX ($n = 1031$, translucent grey points; higher-sampled configurations accordingly appear darker) and validated with wind tunnel tests of 3D-printed wing shapes distributed across the range (white squares). (*b*) Experimental wings (photo, left) were tested at an 80% scale from the numerical wings (front view of figure 1*b*, right). (*c*) Planform views of the 3D-printed wing shapes corresponding in location/arrangement to the white squares in (*a*) and the plots in (*d*) and (*e*). Wing shapes in (*b*) and (*c*) are described by (elbow angle, wrist angle). (*d*) MachUpX predicted the lift force within the expanded uncertainty range at low angles of attack. (*e*) The numerical results for lift and pitching moment lie within the expanded uncertainty range on both variables. The error bars represent the expanded uncertainty range, approximately a 95% confidence interval.

(figure 2*a–c*). The wing shapes are identical to those tested in MachUpX due to a feature that outputs the DXF files for a specified wing shape [26]. These files were prepared into a 3D model and 3D printed on a CONNEX500 printer in a rigid plastic (VeroWhitePlus). We printed half-span wing-body models at 80% scale to ensure that the largest wingspan only extended to 71% of the tunnel width. The printed wings were lightly sanded to minimize surface roughness.

The final wings were tested in the University of Michigan 2ft-by-2ft low-speed wind tunnel at 12.5 m s^{-1} (electronic supplementary material, figures S1 and S2). This enforced a constant Reynolds number (*Re*) between the experimental and numerical tests of approximately 1.4–1.5 × 10^5 based on the maximum mean chord for the wing-body specimen. The wings were mounted to the top of the wind tunnel on a six-axis load cell (ATI Delta) that sampled at 4 kHz for 45 s. There was a 0.5-inch gap between the body and the tunnel edge. The load cell was installed on a rotary table (Parker 30012-S) connected to a motor (VEXTA PK266-03B) and a VELMAX motor controller. This installation method used the reflection plane methodology and blockage constraints were neglected due to the minimal size of the wings relative to the tunnel test section [37]. Using a custom MATLAB script, we performed an angle of attack sweep from 0°to 24° (Δ2°), 25° to 1° (Δ2°), 0° to −3° (Δ1°) and −4° to −20° (Δ2°).

Finally, to investigate the differences between the wind tunnel and numerical results, we fit a first-order linear model to the numerical and experimental results from the nine tested wing shapes for the lift and pitching moment data, respectively, with the elbow, wrist, angle of attack (or lift for the pitching moment model) and method as the dependent variables.

3. Results

3.1. MachUpX validation

The MachUpX lift and pitching moment results fell within the expanded experimental uncertainty range for low angles of attack (figure 2*d*,*e*) [38]. Disregarding the expanded

uncertainty range, there was an average absolute error in the lift and pitching moment of 0.08 and 0.04 at 0°, respectively. Note this is largely manifested by MachUpX underpredicting the lift for lower wrist angles and higher elbow angles (figure 2*d*, configurations 6, 8 and 9). By 5°, the error in both metrics more than doubled. We found that there was no significant effect of methodology (experimental or numerical) on the predicted coefficient of regressions for either the elbow or the wrist. However, there was a significant effect of methodology (p-value < 0.001) on the predicted coefficient of regression for the angle of attack for both the lift and pitching moment models. Specifically, at high angles of attack MachUpX either did not converge, or under predicted the magnitude of lift and pitching moment, likely due to more stalled regions. Informed by these outcomes, the rest of our analyses were limited to angles of attack less than 5°.

3.2. Lift force and pitching moment production

With the outputs from MachUpX, we evaluated the lift and pitching moment at a constant 0° angle of attack for all wing-body configurations (figure 3*a* and *b*). We found that the majority of the configurations produced a negative (nose-down) pitching moment and a positive lift force. Figure 3*a*,*b* reveals that wings with high elbow and low wrist angles had the highest lift and lowest pitching moment, representing the highest absolute loading condition. Unexpectedly, we found that these highly loaded wing-body configurations did not have the highest wing area (total or projected) but instead had the most positive twist angle at the wingtips (figure 3*c*). Positive twist known as wash-in, occurs when the wingtips are at a higher angle of attack than the wing root. Traditional aircraft are designed with wash-out so that the wing root will stall before the wing tip, which improves the handling characteristics of the aircraft [39]. The importance of twist in lift and pitching moment production is supported by a previous experimental study that demonstrated that active wing twist morphing alone provides effective longitudinal control of a tailless aircraft [40]. For the tested configurations, we found that wash-in was associated with a highly swept wing while the less swept (extended) wings exhibited wing tip wash-out. Although wingtip twist was a good predictor of the developed forces and moments, models informed by the elbow and wrist also successfully predicted the developed lift (conditional R^2 of 0.90) and pitching moment (conditional R^2 of 0.98) (see the electronic supplemental material for further details). The good model fit suggests that an engineered joint-driven morphing wing could provide a reliable method for controlling the lift and pitching moment in flight, similar to twist control.

Our results have important consequences for estimations of aerodynamic forces on live gliding birds. Specifically, the wing area may not be an effective metric to differentiate between the lift and pitching moment produced by different wing shapes used by the same bird (figure 3*c*). Instead, if they can be obtained the wingtip twist and sweep angle can provide improved metrics.

3.3. Longitudinal stability and balance

Next, we assessed longitudinal balance and stability using the pitch-stability derivative (slope) and zero-lift pitching moment (y-intercept) from the linear model:

$$C_{m_{\text{morph}}} = \frac{dC_{m_{\text{morph}}}}{dC_{L_{\text{morph}}}} C_{L_{\text{morph}}} + C_{m_{\text{morph},L=0}}. \tag{3.1}$$

A flyer is statically stable if the pitch-stability derivative is negative, and a flyer can be balanced while statically stable if the zero-lift pitching moment is positive.

3.3.1. Longitudinal static stability

First, we evaluated the static stability, which requires that a stable glider perturbed from its equilibrium by an external disturbance (figure 3*d*) will develop a change in pitching moment with an opposite sign to the change in the lift force. This returns the glider towards its equilibrium. We found that all the investigated wing-body configurations had entirely negative pitch-stability derivatives and thus were statically stable (figure 3*e*). The magnitude of the static stability was higher for more folded wing configurations.

Next, we evaluated the traditional aircraft static margin metric which is equal and opposite to the pitch-stability derivative:

$$\text{static margin} = -\frac{dC_{m_{\text{morph}}}}{dC_{L_{\text{morph}}}} = \frac{x_{\text{CG}} - x_{\text{NP}}}{c_{\max}}. \tag{3.2}$$

Where x_{CG} is the location of the centre of gravity and x_{NP} is the neutral point of the wing-body configuration, which is the location where the pitching moment is independent of the angle of attack. The negative pitch-stability derivatives (positive static margins) for all our tested configurations indicated that x_{NP} is substantially aft of the body quarter-chord. When we considered the magnitude of the change, our results revealed that joint-driven wing morphing permits a maximum static margin shift of 24% of $c_{\max}$, or approximately 5.1 cm. Moreover, if the gull-inspired wing-body x_{CG} was relocated between 4.1 and 9.2 cm behind the shoulder joint, this sizable static margin shift would allow the glider to shift between stable and unstable configurations. Further, we found that joint-driven wing morphing provides an effective method to control the static margin as the elbow and wrist angles were good predictors of the pitch-stability derivative (conditional $R^2 = 0.83$). In any case, this large static margin shift would result in significantly different handling qualities between configurations, which is usually an undesirable condition for human pilots [23].

This analysis assumes a fixed x_{CG}, but in actuality morphing a wing can cause the centre of gravity to shift. To estimate an approximate x_{CG} shift associated with joint-driven wing morphing, we investigated the solid 3D-printed wings and found a maximum backwards shift of 1.3 cm. Note that this will not necessarily be comparable to an engineered morphing wing because the weight distribution will depend on the manufactured design. However, the x_{CG} shift for a real bird wing-body is likely smaller than the 3D-printed wings due to the lightweight nature of feathers compared to the musculoskeletal system and body. To obtain an approximate estimate of the static margin shift, we assumed that the x_{CG} moves opposite to the x_{NP}. This situation would reduce the maximum static margin shift to 3.8 cm (18%). Note that we non-dimensionalized the static margin using $c_{\max}$, but traditional static margin analyses use the mean aerodynamic chord which will be smaller than $c_{\max}$. In all, we expect

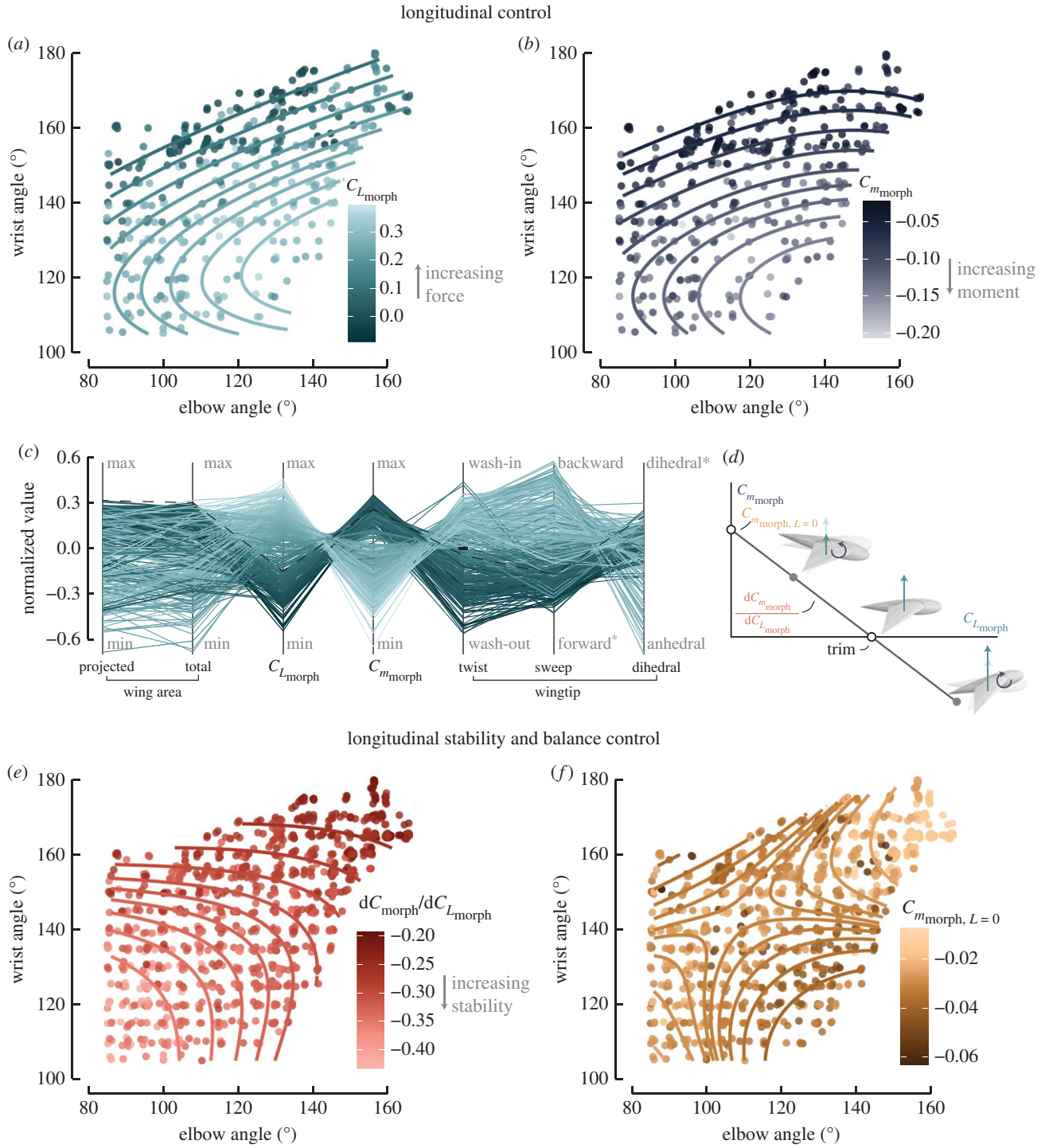

Figure 3. Joint-driven wing morphing provides a reliable method to control the lift, pitching moment and static stability characteristics. (*a*,*b*) Constant lift and pitching moment contour lines overlaid on the numerical results at 0° angle of attack ($n = 414$) highlight a region of high magnitude lift and pitching moment. (*c*) Normalized geometric properties, centred on 0° twist angle (black line). The black dashed line represents the wing configuration with the maximum projected wing area. The colour scheme is based on the normalized value of $C_{L_{morph}}$. (*d*) Longitudinal static stability can be quantified with the zero-lift pitching moment and pitch-stability derivative. (*e*,*f*) Constant pitch-stability derivative and constant zero-lift pitching moment contour lines overlaid on the results obtained from all wings that converged at more than four independent angles of attack ($n = 1012$).

that our calculated static margin shift of 18% represents a conservative estimate.

3.3.2. Longitudinal balance

Next, we investigated the longitudinal balance condition which ensures that while in trimmed flight a glider can create sufficient lift to support its weight when there is no net moment (mathematically represented by a positive *x*-intercept of equation (3.1), figure 3*d*). Because we require a negative slope for static stability, this in turn requires the *y*-intercept or zero-lift pitching moment to be positive. We found that none of our wing-body configurations had a positive zero-lift pitching moment (figure 3*f*). As a result, a gull-inspired wing-body with the wings aligned following our convention could not be balanced at 0° while flying in a stable condition. This result is identical to a positively cambered aircraft wing which has a negative zero-lift pitching moment [22].

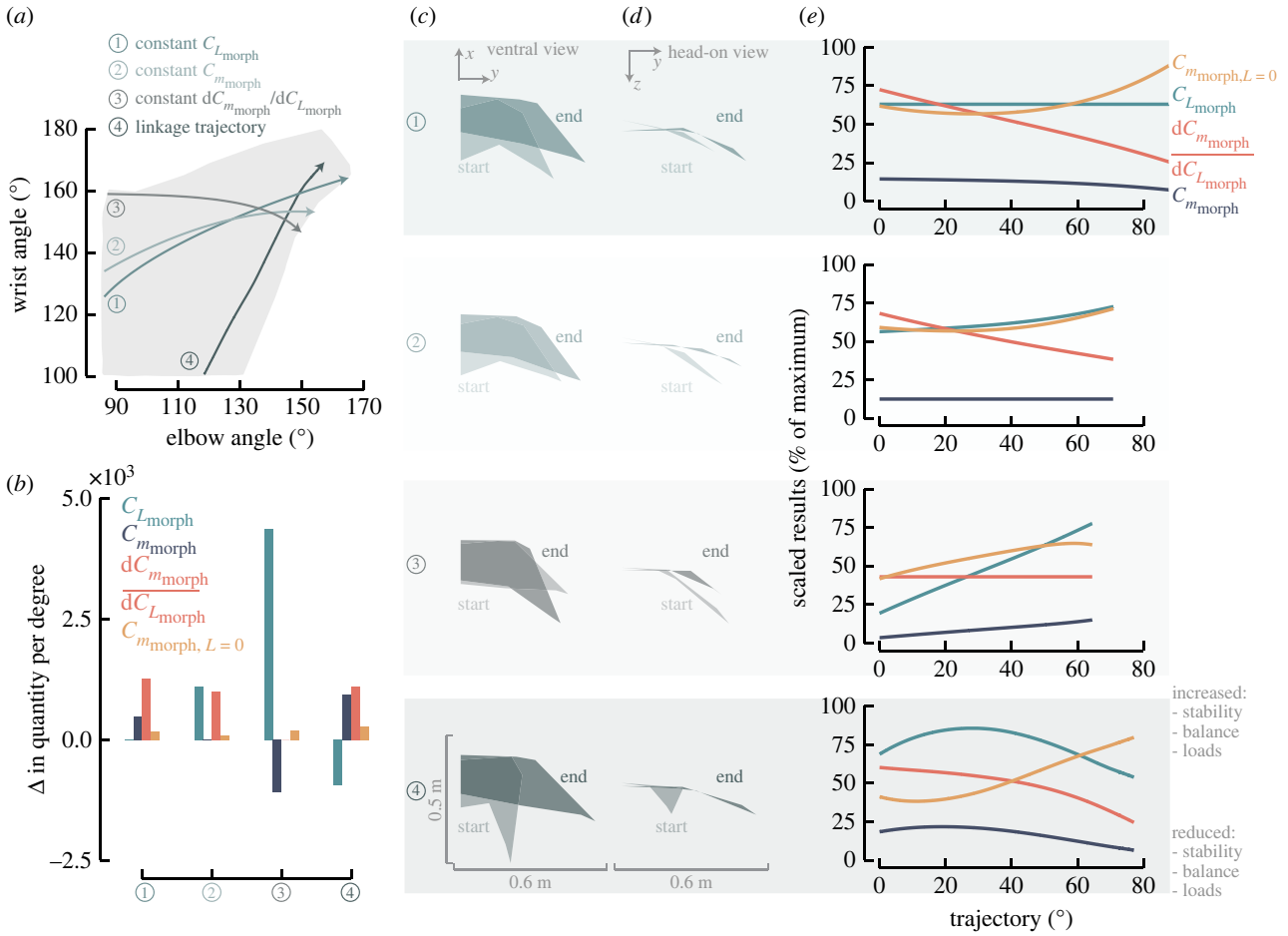

Figure 4. Constant joint extension trajectories allow variable longitudinal control strategies. (*a*) The entire range of motion investigated (shaded region) overlaid with the four investigated trajectories: (1) constant lift force, (2) constant pitching moment, (3) constant pitch-stability derivative, and (4) linkage trajectory. (*b*) The total control effectiveness of the trajectory (*y*-axis) is defined as the change in a parameter between the start and end per degree of extension along the entire trajectory arc length. Planform view (*c*) and head-on view (*d*) of the wing shapes at the start of each trajectory overlaid with the shapes at the end. (*e*) The instantaneous control effectiveness of each longitudinal quantity, represented by the instantaneous slope at each point, is highly variable. Each quantity is scaled between its absolute minimum and maximum based on the results at 0° angle of attack; 0% represents the lowest loads, least stable and least balanced configuration.

Furthermore, our results showed that the elbow and wrist would not provide a reliable method to control the trim position because they were poor predictors of the zero-lift pitching moment (conditional $R^2 = 0.42$). However, a horizontal tail with control surfaces could be added to gain control. Interestingly, unlike fixed-wing aircraft, birds not only have a controllable horizontal tail, but they also can rotate their wing about their shoulder joint. This is especially relevant because birds are capable of sustained flight without their tails, possibly suggesting an alternative method can be used to maintain trimmed flight [4]. It follows that to have controllable, balanced flight for the wing-body configurations investigated, it will be necessary to investigate the possible roles of both a controllable horizontal tail and a controllable shoulder angle.

4. Discussion

Joint-driven wing morphing creates a two-dimensional morphing space (figure 4*a*, shaded region) that encompasses a wide variety of aerodynamic properties available to a single wing. In flight, a joint-driven morphing wing can follow any continuous joint trajectory through this space. We defined a joint trajectory as a specific set of elbow and wrist angles obtained by following any continuous line within the shaded region of figure 4*a*, and a joint extension trajectory as a specific subset of joint trajectories that progress from left to right in figure 4*a*. Note that it is also possible to implement these trajectories in reverse (flexion), however in this work we focus on the effects of extension alone. Each specific joint extension trajectory will be associated with differing gradients in aerodynamic properties where gradients can be visualized by considering the contour lines in figure 3*a*, *b*, *e* and *f*.

To identify joint extension trajectories that could be useful for a gull-inspired morphing UAV, we examined four unique trajectories at a fixed 0° angle of attack while assuming a quasi-steady extension that neglects any unsteady aerodynamic effects (figure 4*a*). The first three trajectories were selected by individually extracting constant contour lines from the lift (number 1), pitching moment (number 2) and pitch-stability derivative models (number 3) (figure 4*a*). The final trajectory considered is the linkage trajectory (number 4) which is the set of coupled elbow and wrist angles that are provided by the mechanical advantage of the gull wing's six-bar linkage system (figure 4*a*) [16,17]. These angles were determined in a previous study by fixing the

humeral head of a specimen's wing and manually applying a point force within an approximate x–y plane (figure 1) to a point on the wrist; this causes both the elbow and wrist joints to extend due to the linkage coupling [17]. This approach allows us to extract the kinematics of the coupled linkage system that is caused by the displacement of a single point, the point on the wrist in this case. Finally, we visualized the wing shape at the start and end of each trajectory from the ventral view (figure 4*c*) and head-on view (figure 4*d*).

We found that both the constant lift and constant pitch-stability derivative trajectories decoupled stability characteristics from load production. First, the constant lift trajectory (figure 4*a*, number 1) created the highest absolute change in the pitch-stability derivative, exhibiting a linear response ($R^2 > 0.99$) throughout the extension (figure 4*b*,*e*). This linear trend indicates that the control effectiveness remains constant, removing the need for a controller to know the exact position of the wing. In addition, this trajectory had a minimal effect on the pitching moment, where the instantaneous control effectiveness (instantaneous slope from figure 4*e*) of the pitching moment was below 5×10^{-4} per degree until over halfway extended but increased as the wing neared maximum extension. In all, extension along the first half of the constant lift trajectory would allow a simple trajectory for a morphing UAV to adjust its static margin without affecting the lift or pitching moment. This extension trajectory could allow a gull-inspired morphing UAV to shift from a stable to an unstable configuration without affecting its longitudinal position or orientation. Decreasing static stability may be useful when a flight environment becomes gustier because lower static stability reduces the strength of the inherently developed pitching moment and may reduce path oscillations [5]. As a result, this morphing trajectory may allow an active form of gust rejection by maintaining the desired altitude and elevation angle.

The second trajectory that decouples stability from load production is the constant pitch-stability derivative trajectory (figure 4*a*, number 3). This extension trajectory created a large magnitude increase in lift and decrease in pitching moment both with linear responses ($R^2 > 0.99$) throughout extension (figure 4*b*,*e*). This trajectory acts similar to a traditional symmetric flap deflection because a downward flap deflection increases lift and creates a nose-down pitching moment, which can be counteracted with a controllable horizontal tail. Thus, as with flaps this extension trajectory could be used to steepen the approach angle during landing. Also similar to flaps that do not change the overall wing area, this trajectory avoids the undesirable change to an aircraft's handling qualities that is caused by a static margin shift [23]. However, because the relationship between lift and pitching moment is directly affected by the location of x_{CG}, a successful implementation of this morphing trajectory in a gull-inspired morphing UAV will need to include a detailed trade-off study investigating the most beneficial placement of x_{CG}.

Our results showed that minor variations off the identified trajectories re-couples the stability and loading characteristics. Consider the constant pitching moment trajectory (figure 4*a*, number 2) which appears to be slightly askew from the constant lift trajectory (figure 4*a*, number 1). Yet, the constant pitching moment trajectory has a strong nonlinear coupling between the developed lift and static stability (figure 4*b*,*e*). Thus, for a UAV to gain the discussed benefits from the two decoupled trajectories the joint angle control will need to be precise, which increases the challenge of manufacturing an effective joint-driven morphing wing.

Finally, we investigated extension along the linkage trajectory (figure 4*a*, number 4) and found that this extension does not cause the largest change to any individual parameter but does cause the largest magnitude change across all parameters compared to the other investigated trajectories. Interestingly, there was a nonlinear response, such that the instantaneous control effectiveness differs substantially from the total control effectiveness (figure 4*e*,*b*). Specifically, at the start of the extension trajectory $C_{L_{morph}}$ increases by 6.3×10^{-3} per degree and $C_{m_{morph}}$ decreases by 2.2×10^{-3} per degree, increasing the absolute load on the wing. Near the end of the extension trajectory $C_{L_{morph}}$ decreases by 4.7×10^{-3} per degree and $C_{m_{morph}}$ increases by 2.2×10^{-3} per degree, decreasing the absolute load on the wing. Thus, extension alone allows a method to both increase and decrease aerodynamic loads, solely dependent on the wing's position along the extension. Note that these instantaneous control effectiveness values are a larger magnitude compared to those obtained by all other investigated trajectories (figure 4*b*,*e*). The strong variability in the response possibly allows the linkage trajectory to serve many different functions in flight such as initiating and maintaining complex manoeuvres. Moreover, due to the mechanical advantage of the linkage system, following this trajectory requires input from only a single actuator which would simplify the manufacturing process of such a wing. However, the lift and pitching moment are strongly coupled to the balance and stability characteristics for the linkage trajectory. As such, flight control using joint-driven wing morphing along the linkage trajectory would be undesirable for human pilots without an additional controller to account for the shifting static margin.

There are few comparable-sized engineered morphing wing aircraft with published longitudinal characteristics. One great example is a goshawk-inspired drone with a maximum wing span (1.05 m) that is 87% of the scale of our largest wing (1.21 m) [12]. This aircraft saw a minimal change in the lift and pitching moment produced between a swept and extended position (with a furled tail) around 0° but, at higher angles of attack the extended wing had substantially higher loads with an absolute variation up to roughly 0.5 in C_L and 0.4 in C_m. Note that C_m was non-dimensionalized by the mean aerodynamic chord which is smaller than c_{max} and thus our range of pitching moment cannot be compared directly. Our morphing wing-body numerical results showed an absolute variation of 0.48 in $C_{L_{morph}}$ and 0.18 in $C_{m_{morph}}$ at 0°. Further investigation of our experimental results indicated that the absolute variation remains relatively constant across the investigated angles of attack with the range only beginning to reduce below −5°. This suggests that a joint-driven morphing wing UAV may effectively provide lift and pitching moment control across a broader range of angles of attack when compared with planar sweep-only morphing.

The preceding discussions of longitudinal stability and balance have assumed that the gull-inspired morphing UAV would be controlled with open-loop stability (as is done when a glider is statically stable). Instead, it is possible to

use closed-loop stability to successfully fly while in an unstable configuration [23]. For the gull-inspired morphing UAV, the x_{CG} would have to be shifted backwards by over 9.2 cm from the body quarter-chord to render the entire range of motion unstable. In this configuration, the pitch-stability derivative will be positive and thus, a negative zero-lift pitching moment would permit a trimmed position. In traditional aircraft design this is called relaxed static stability. Such an aircraft benefits from improved drag performance and manoeuvrability characteristics but requires a high degree of control to avoid the potentially serious consequences of an unstable response to external inputs such as gusts [23]. Our current results cannot comment on if live birds use open-loop or closed-loop control, but for a gull-inspired morphing UAV, closed-loop control offers an alternative to installing a horizontal tail. In this case, the trim position would still need an effective control method. This control could possibly be provided by the shoulder angle similar to hang gliders [4,22].

It is important to note that our previous study of real prepared gull wings found the opposite relationship between elbow angle and the pitch-stability derivative compared to the current rigid wing results [5]. We expect that differences between the two studies may be caused by feather flexibility, feather porosity, different wing alignments and/or the inclusion of wing-body interaction effects within the current study. Further investigation to understand the differences between a rigid 3D-printed wing shape and a real gull wing will be necessary.

To this end, many assumptions were required to allow a targeted analysis of the effects of elbow and wrist morphing and will require investigation in future studies to approach a general understanding of how birds fly. For example, in this study we did not include variations in velocity or *Re*. Birds use an intermediate *Re* and it is therefore possible that shifting into a lower or higher regime could have a measurable effect on the longitudinal characteristics of an avian-inspired wing [19]. Additionally, it will be necessary to evaluate the coupled role of shoulder joint control with elbow and wrist morphing to develop a holistic understanding of flight control due to avian wing morphing. Further, our work assumed quasi-steady extension, however in reality birds can manipulate their joints very quickly which could result in induced flow along all major directions. A detailed mechanistic study is warranted in the future to determine the presence and the role of specific unsteady aerodynamic effects. Finally, we only investigated a single species, but birds have a broad range of species diversity, each of which may offer unique insights on how to efficiently design UAVs. In particular, we expect different control effectiveness values between different bird species due to variable wing range of motion, linkage structures and overall geometry [17–19].

5. Conclusion

We investigated the potential benefits of gull-inspired joint-driven wing morphing for future UAV applications. First, we determined a set of simplified wing shapes across the range of motion of the elbow and wrist used by gliding gulls. Next, we used a numerical general lifting-line model (MachUpX) validated with wind tunnel experiments to determine the longitudinal characteristics of the wing-body configurations. Our results showed that wings with the highest load production had low wrist and high elbow angles and were associated with wing tip wash-in. Additionally, although the inherent response to an external disturbance for all wing-body configurations was stable, we found that a controllable horizontal tail or shoulder angle would be necessary to successfully provide open-loop control. Importantly, we found that the elbow and wrist angle could provide a reliable method to control the lift, pitching moment and overall static margin but would not be sufficient to control the zero-lift pitching moment alone.

Our study revealed that the two-dimensional morphing space allowed by the elbow and wrist joints permits a wide variety of flight control strategies. In particular, we identified two trajectories that decoupled longitudinal static stability and longitudinal load production. One trajectory (figure 4*a*, number 1) linearly adjusts static stability without affecting the load production and the other (figure 4*a*, number 3) linearly adjusts the lift and pitching moment without affecting stability, in a manner similar to an aircraft flap that does not change the wing area. Moreover, the identified linear response is highly advantageous for a simplified controller design. However, we found that a unique but similar trajectory (figure 4*a*, number 2) re-couples the loads and stability, suggesting that precise control of the elbow and wrist would be necessary to realize these aerodynamic benefits in a UAV. Finally, the linkage trajectory (figure 4*a*, number 4) afforded by the gull's musculoskeletal linkage system yielded the highest instantaneous control effectiveness of all our investigated trajectories and represents a simple actuation trajectory that can quickly adjust the longitudinal characteristics. However, the load production and stability are highly coupled for this trajectory and other control mechanisms would be required to negate this effect. In all, investigation of these unique trajectories highlights the multifunctional capabilities of gull-inspired joint-driven wing morphing.

Despite the identified aerodynamic benefits of a joint-driven morphing wing, a major challenge for any bioinspired UAV is to design an efficient actuation mechanism that can realize the proposed benefits in practice. In the past, a non-planar wing design that was indirectly inspired by gulls, the HECS wing (discussed in the Introduction) was shown to yield minimal aerodynamic benefits when it was actively morphed into its furled configuration [41] despite promising rigid model results [20]. This emphasizes the multidisciplinary challenges associated with effective morphing wing design. Successful implementation of gull-inspired joint-driven morphing wings will require detailed structural analyses, flight tests and multidisciplinary investigations to determine if the benefits identified within this study could effectively and efficiently be realized in a morphing wing UAV.

Do the benefits provided by joint-driven wing morphing outweigh engineered morphing wing designs? Our results show that gull-inspired joint-driven wing morphing creates a similar magnitude of control effectiveness as an equivalent aircraft with a sweeping mechanism, but with the added multifunctional capabilities permitted by the variable joint extension trajectories. This is especially promising because we found that a joint-driven morphing wing can produce a similar aerodynamic response to traditional flaps but would not be limited to this singular functionality. Combined with future multidisciplinary investigations, we expect that gull-inspired joint-driven wing morphing could provide a future

generation of UAVs the unique ability to adapt on the fly by morphing along the specific joint trajectory that realizes the desired aerodynamic characteristics.

Data accessibility. All data and custom codes reported in this paper have been deposited in public repositories identified within: https://doi.org/10.6084/m9.figshare.c.5275490 [42].

Authors' contributions. C.H., V.B.B. and D.J.I. designed the study. C.D.G. and D.F.H. developed MachUpX and supported implementation of the gull wing models. C.H. collected and analysed the experimental and numerical results. V.B.B. and C.H. collected the specimen manipulation data. C.H. wrote the manuscript. All authors edited the manuscript.

Competing interests. The authors declare no conflict of interests.

Funding. This work is supported in part by the US Air Force Office of Scientific Research under grant no. FA9550-16-1-0087, titled 'Avian-Inspired Multifunctional Morphing Vehicles' monitored by Dr B.L. Lee and in part by the National Science Foundation under grant no. 1935216. C.H. is further supported by a PGS-D through the Natural Sciences and Engineering Research Council of Canada (NSERC) and the Francois-Xavier Bagnoud Fellowship awarded by FXB International through the University of Michigan Department of Aerospace Engineering.

Acknowledgements. The authors would like to thank Prof. L.P. Bernal for his input on the experimental methodology.

References

1. Pennycuick CJ. 1968 A wind-tunnel study of gliding flight in the pigeon *Columba livia*. *J. Exp. Biol.* **49**, 509–526. (doi:10.1242/jeb.49.3.509)
2. Lentink D *et al*. 2007 How swifts control their glide performance with morphing wings. *Nature* **446**, 1082–1082 (doi:10.1038/nature05733)
3. Valasek J. 2012 *Morphing aerospace vehicles and structures*. New York, NY: John Wiley & Sons.
4. Thomas ALR, Taylor GK. 2001 Animal flight dynamics I. Stability in gliding flight. *J. Theor. Biol.* **212**, 399–424. (doi:10.1006/jtbi.2001.2387)
5. Harvey C, Baliga VB, Lavoie P, Altshuler DL. 2019 Wing morphing allows gulls to modulate static pitch stability during gliding. *J. R. Soc. Interface* **16**, 20180641. (doi:10.1098/rsif.2018.0641)
6. Barbarino S, Bilgen O, Ajaj RM, Friswell MI, Inman DJ. 2011 A review of morphing aircraft. *J. Intell. Mater. Syst. Struct.* **22**, 823–877. (doi:10.1177/1045389x11414084)
7. Mintchev S, Floreano D. 2016 Adaptive morphology: a design principle for multimodal and multifunctional robots. *IEEE Robot. Autom. Mag.* **23**, 42–54. (doi:10.1109/MRA.2016.2580593)
8. Wickenheiser AM, Garcia E. 2008 Optimization of perching maneuvers through vehicle morphing. *J. Guid. Control Dyn.* **31**, 815–823. (doi:10.2514/1.33819)
9. Lissaman P. 2009 Effects of turbulence on bank upsets of small flight vehicles. In *47th AIAA Aerospace Sciences Meeting including The New Horizons Forum and Aerospace Exposition, 5–8 January, Orlando, FL*. Reston, VA: AIAA. (doi:10.2514/6.2009-65)
10. Orr MW, Rasmussen SJ, Karni ED, Blake WB. 2005 Framework for developing and evaluating MAV control algorithms in a realistic urban setting. In *American Control Conf., 2005. Proc. 2005, 8–10 June, Portland, OR*, pp. 4096–4101. New York, NY: IEEE. (doi:10.1109/ACC.2005.1470619)
11. Chang E, Matloff LY, Stowers AK, Lentink D. 2020 Soft biohybrid morphing wings with feathers underactuated by wrist and finger motion. *Sci. Robot.* **5**, eaay1246. (doi:10.1126/scirobotics.aay1246)
12. Ajanic E, Feroskhan M, Mintchev S, Noca F, Floreano D. 2020 Bioinspired wing and tail morphing extends drone flight capabilities. *Sci. Robot.* **5**, eabc2897. (doi:10.1126/scirobotics.abc2897)
13. Abdulrahim M, Lind R. 2004 Flight testing and response characteristics of a variable gull-wing morphing aircraft. In *AIAA Guidance, Navigation, and Control Conf. and Exhibit, 16–19 August, Providence, RI*. Reston, VA: AIAA.
14. Di Luca M, Mintchev S, Heitz G, Noca F, Floreano D. 2017 Bioinspired morphing wings for extended flight envelope and roll control of small drones. *Interface Focus* **7**, 20160092. (doi:10.1098/rsfs.2016.0092)
15. Paranjape AA, Chung S-J, Selig MS. 2011 Flight mechanics of a tailless articulated wing aircraft. *Bioinspir. Biomim.* **6**, 026005. (doi:10.1088/1748-3182/6/2/026005)
16. Stowers AK, Matloff LY, Lentink D. 2017 How pigeons couple three-dimensional elbow and wrist motion to morph their wings. *J. R. Soc. Interface* **14**, 20170224. (doi:10.1098/rsif.2017.0224)
17. Baliga VB, Szabo I, Altshuler DL. 2019 Range of motion in the avian wing is strongly associated with flight behavior and body mass. *Sci. Adv.* **5**, eaaw6670. (doi:10.1126/sciadv.aaw6670)
18. Harvey C, Baliga VB, Altshuler DL, Inman DJ. 2019 Pitch control effectiveness of the avian elbow and wrist via a numerical lifting line analysis. In *AIAA Scitech 2019 Forum, 7–11 January, San Diego, CA*. Reston, VA: AIAA. (doi:10.2514/6.2019-0853)
19. Harvey C, Inman DJ. 2020 Aerodynamic efficiency of gliding birds vs. comparable UAVs: a review. *Bioinspir. Biomim.* **16**, 031001. (doi:10.1088/1748-3190/abc86a)
20. Lazos B, Visser K. 2006 Aerodynamic comparison of hyper-elliptic cambered span (HECS) wings with conventional configurations. In *24th AIAA Applied Aerodynamics Conf., 5–8 June, San Francisco, CA*, pp. 1–18. Reston, VA: AIAA. (doi:10.2514/6.2006-3469)
21. Taylor G, Thomas A. 2014 *Evolutionary biomechanics*. Oxford, UK: Oxford University Press.
22. Anderson Jr JD. 1989 *Introduction to flight*. New York, NY: McGraw-Hill Higher Education.
23. Pamadi BN. 2004 *Performance, stability, dynamics, and control of airplanes*. Reston, VA: American Institute of Aeronautics & Astronautics.
24. Meyers RA, Mathias E. 1997 Anatomy and histochemistry of spread-wing posture in birds. 2. Gliding flight in the California gull, *Larus californicus*: a paradox of fast fibers and posture. *J. Morphol.* **233**, 237–247. (doi:10.1002/(SICI)1097-4687(199709)233:3<237::AID-JMOR3>3.0.CO;2-0)
25. Williamson CJ, Spelt A, Windsor SP. 2020 Bird-inspired velocity optimization for UAVs in the urban environment. In *AIAA Scitech 2020 Forum, 6–10 January, Orlando, FL*, p. 1948. Reston, VA: AIAA. (doi:10.2514/6.2020-1948)
26. AeroLab. 2020 *Machupx: fast and accurate aerodynamic modelling using lifting-line theory*. See https://www.github.com/usuaero/MachUpX.
27. Reid JT, Hunsaker DF. 2020 A general approach to lifting-line theory, applied to wings with sweep. *J. Aircr.* **58**, 1287. (doi:10.2514/6.2020-1287)
28. Goates CD, Hunsaker DF. 2021 Practical implementation of a general numerical lifting-line method. In *AIAA Scitech 2021 Forum, 11–15 & 19–21 January*. Reston, VA: AIAA. (doi:10.2514/6.2021-0118)
29. Hedrick, Tyson L. 2008 Software techniques for two- and three-dimensional kinematic measurements of biological and biomimetic systems. *Bioinspir. Biomim.* **3**, 034001. (doi:10.1088/1748-3182/3/3/034001)
30. Liu T, Kuykendoll K, Rhew R, Jones S. 2006 Avian wing geometry and kinematics. *AIAA J.* **44**, 954–963. (doi:10.2514/1.16224)
31. Bachmann T. 2010 Anatomical, morphometrical and biomechanical studies of barn owls' and pigeons' wings. PhD thesis. RWTH Aachen University, Aachen, Germany.
32. Nachtigall W, Wieser J. 1966 Profilmessungen am Taubenflugel. *Z. Vgl. Physiol.* **52**, 333–346. (doi:10.1007/BF00302288)
33. Carruthers AC, Walker SM, Thomas ALR, Taylor GK. 2010 Aerodynamics of aerofoil sections measured on a free-flying bird. *Proc. Inst. Mech. Eng. Part G J. Aerosp. Eng.* **224**, 855–864. (doi:10.1243/09544100jaero737)
34. Lee S, Choi H. 2017 Characteristics of the alula in relation to wing and body size in the Laridae and Sternidae. *Anim. Cells Syst.* **21**, 63–69. (doi:10.1080/19768354.2016.1266287)
35. Nudds R, Rayner J. 2006 Scaling of body frontal area and body width in birds. *J. Morphol.* **267**, 341–346. (doi:10.1002/jmor.10409)
36. Shepard ELC, Williamson C, Windsor SP. 2016 Fine-scale flight strategies of gulls in urban airflows

indicate risk and reward in city living. *Phil. Trans. R. Soc. B* **371**, 20150394. (doi:10.1098/rstb.2015.0394)

37. Barlow JB, Rae WH, Pope A. 1999 *Low-speed wind tunnel testing*. New York, NY: John Wiley & Sons.
38. Working Group 1 of the Joint Committee for Guides in Metrology (JCGM/WG 1). 2008 Evaluation of measurement data—guide to the expression of uncertainty in measurement. Report no. JCGM 100:2008. See https://www.bipm.org/documents/20126/2071204/JCGM_100_2008_E.pdf/cb0ef43f-baa5-11cf-3f85-4dcd86f77bd6.
39. McLean D. 2012 *Understanding aerodynamics: arguing from the real physics*. New York, NY: John Wiley & Sons.
40. Guiler R, Huebsch W. 2005 Wind tunnel analysis of a morphing swept wing tailless aircraft. In *23rd AIAA Applied Aerodynamics Conf., 6–9 June, Toronto, Canada*, p. 4981. Reston, VA: AIAA. (doi:10.2514/6.2005-4981)
41. Manzo J, Garcia E. 2010 Demonstration of an in situ morphing hyperelliptical cambered span wing mechanism. *Smart Mater. Struct.* **19**, 025012. (doi:10.1088/0964-1726/19/2/025012)
42. Harvey C, Baliga VB, Goates CD, Hunsaker DF, Inman DJ. 2021 Data from: Gull-inspired joint-driven wing morphing allows adaptive longitudinal flight control. FigShare. (doi:10.6084/m9.figshare.c.5275490)